frontiers | Frontiers in Materials

TYPE Original Research
PUBLISHED 30 October 2024
DOI 10.3389/fmats.2024.1480043

OPEN ACCESS

EDITED BY
Samir Allaoui,
Université de Reims
Champagne-Ardenne, France

REVIEWED BY
M'Hamed Boutaous,
Institut National des Sciences Appliquées de Lyon (INSA Lyon), France
Muammel M. Hanon,
Middle Technical University, Iraq

*CORRESPONDENCE
Yanling Guo,
nefugyl@hotmail.com

RECEIVED 13 August 2024
ACCEPTED 21 October 2024
PUBLISHED 30 October 2024

CITATION
Guo C, Guo Y, Li J, Wang Y and Dai J (2024) Study on the mechanical properties of PES-HmA samples printed by selective laser sintering under various pre-heating conditions.
Front. Mater. 11:1480043.
doi: 10.3389/fmats.2024.1480043

Study on the mechanical properties of PES-HmA samples printed by selective laser sintering under various pre-heating conditions

Chengbo Guo[1,2], Yanling Guo[2]*, Jian Li[2], Yangwei Wang[2] and Jiaming Dai[2]

[1]College of Civil Engineering and Transportation, Northeast Forestry University, Harbin, China, [2]College of Mechatronics Engineering, Northeast Forestry University, Harbin, China

The purpose of this study is to investigate the influence of pre-heating characteristics on the mechanical properties and forming process of selective laser sintering (SLS) printed PES-HmA samples. An experimental setup with four heating tubes was designed to study the pre-heating temperature distribution on the powder bed. The pre-heating temperature distribution on the powder bed was captured using a thermal imaging camera. A method for evaluating pre-heating temperature distribution based on the average and standard deviation of surface temperature was proposed. The heating tube installation position was optimized using a response surface experiment study based on the temperature distribution evaluation. By optimizing the installation position of the tubes, the temperature distribution on the powder bed tends to become uniform. The effect of pre-heating temperature value and distribution on the mechanical properties of the SLS printed PES-HmA samples was also experimentally investigated. The cross sectional microstructure of the printed samples were examined by scanning electron microscope to analyze the layer formation process at different pre-heating temperature. By increasing the pre-heating temperature from 70°C to 100°C, the material diffusion at the layers interface was improved, which made the tensile strength of sample increased by 376%, and the flexural strength increased by 224%.

KEYWORDS

selective laser sintering, PES-HmA, pre-heating, temperature distribution, tensile strength, flexural strength, formation process

1 Introduction

Additive manufacturing, also known as 3D printing, has been employed in various fields to produce customized parts without the use of specific molds or tools (Mantovani et al., 2020). It is becoming increasingly popular due to its superiority in printing lightweight and complex geometries components cost-effectively (Savolainen and Collan, 2020; Abdulhameed et al., 2019). Selective laser sintering (SLS) is an additive manufacturing technique that can create complex and functional parts by selectively melting powders layer by layer using a high power-density laser (Yap et al., 2015; Liang et al., 2022). Prior to the printing process, the powder is pre-heated to a fixed temperature below the melting point,

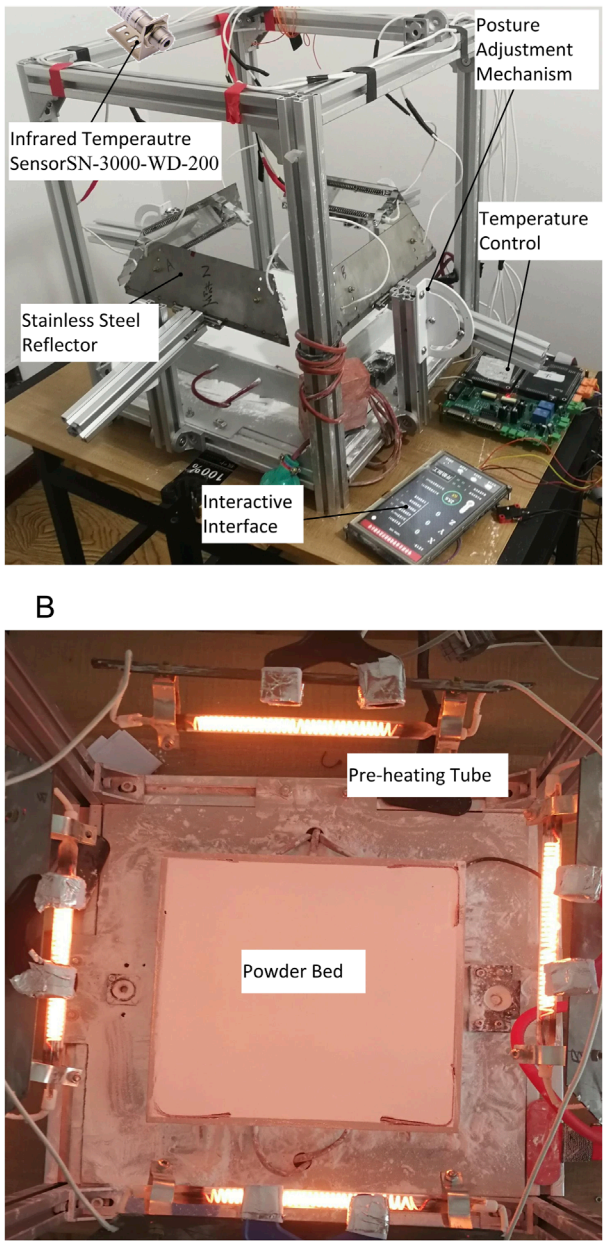

FIGURE 1
Schematic of the designed pre-heating setup: **(A)** experiment setup; **(B)** top view of the setup.

and the melting rate of the powder is accelerated by laser irradiation (Sharma et al., 2020). Polyether sulfone hot melt adhesive (PES-HmA), which is a kind of polymeric composite material with a wide heat treatment window, is widely used as SLS printing material due to its excellent thermoplastic properties (Yuan et al., 2019; Parandoush and Lin, 2017). The mechanical properties of the printed polymer part lack stability and reliability, which limited the application of PES-HmA in SLS printing (Jatti et al., 2024).

In order to understand the forming principle of SLS, many researches have been conducted to study the binding mechanism and laser heating process (Strano et al., 2011). Based on the bonding mechanism, Kruth et al. classified the SLS technology into solid state sintering, chemical induced binding, partial melting, and full melting (Kruth et al., 2005). Compared to components fabricated at room temperature, the fabricated component would have higher ultimate tensile strength and ductility by pre-heating the powders with elevated temperature (Martinez et al., 2019). Savalani et al. verified the importance of the pre-heating process in improving the quality of produced surface, and the low layer thickness was conducive to obtaining a smoother and flatter machined surface (Savalani and Pizarro, 2016). Antonov et al. experimentally and theoretically studied the dynamics of laser induced heating process of polymer particles, they found that the polymer particles could be effectively sintered by the fine melting of the particle surface (Antonov et al., 2020). Yang et al. proposed a method to pre-heating powder by lamp radiation and tropical heat conduction, and the forming quality can be improved by constructing uniform temperature field (Yang et al., 2022).

Thermal model is a good way to understand the mechanism of laser powder bed fusion mechanism (Tangestani et al., 2021). By constructing a transient thermal model using the finite element method, Papadakis et al. investigated the energy consumption of building chamber pre-heating, base plate heating, and laser pre-scan heating respectively (Papadakis et al., 2017). It was found that the pre-heating efficiency was affected by the size of parts being fabricated, and the laser pre-scanning heating would be more efficient when machining small size parts. Landau et al. constructed a numerical model of the build chamber of an ARCAM Q20+ machine, evaluated the energy required to pre-heating the powder to the desired temperature, and assessed the heat transfer effect during the pre-heating process (Landau et al., 2020). The model was verified by real-time monitoring of the printing chamber temperature using 9 thermocouples fixed on the stainless steel start plate. Through the experimental and numerical study of the composite consolidation process, Zhilyaev et al. presented an advanced finite element numerical model which has a good performance in simulating the consolidation process of additive manufacturing continuous fiber composite parts (Zhilyaev et al., 2022). The numerical simulation enables the printing of complex parts without expensive prototyping iterations.

The printing temperature plays an important role in guarantee the mechanical properties of printed parts (Chen et al., 2023). In order to control the temperature difference on the powder surface, by utilizing an infrared camera to monitor the powder bed surface temperature, Phillips et al. proposed a feed-forward laser fluence controller to adjust the laser power in real time based on a dynamic sintering model (Phillips et al., 2018). The result shows that the post-sintering temperature uniformity was improved by 57%, and the deviation of the printed samples' flexural strength was reduced by 45%. Liu et al. reduced the cracks generated during laser processing of yttria stabilized zirconia ceramic by pre-heating the powder to a high temperature (Liu et al., 2015). Both mechanical properties and surface roughness were influenced by the sintering process (Bai et al., 2016; Singh et al., 2013). Ling et al. investigated the influence of ambient temperature and densification on the mechanical properties of sintered specimens, and they found that the average porosity ratio in the specimen can be reduced by improving the ambient temperature, which is beneficial for enchaning its tensile strength (Ling et al., 2018).

10.3389/fmats.2024.1480043

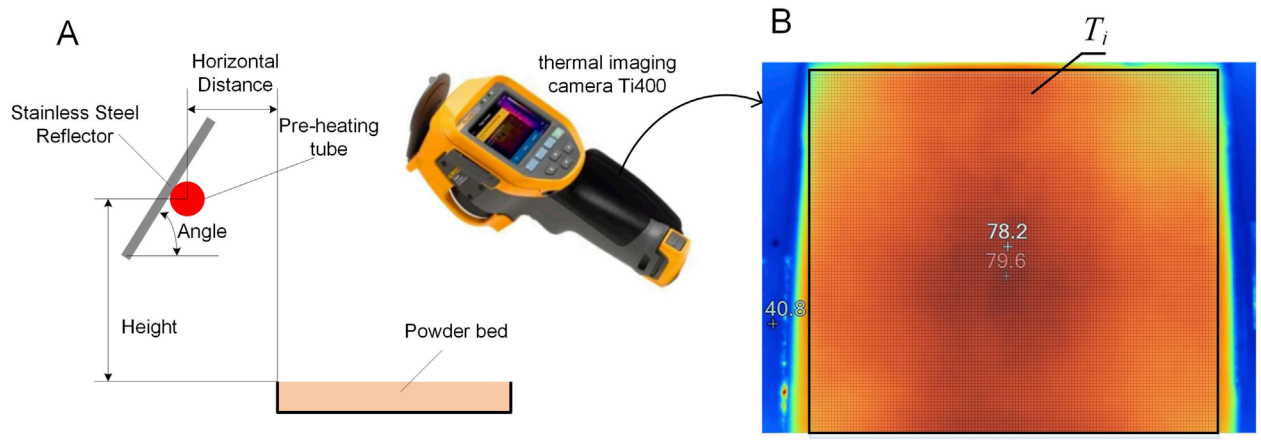

FIGURE 2
The schematic diagram of **(A)** adjustable parameters for the mounting position of heating tubes and **(B)** Ti400 captured thermal image.

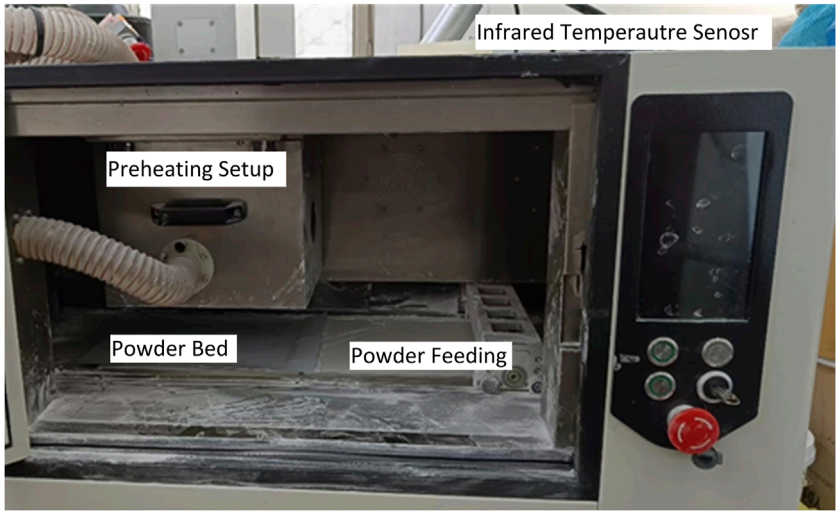

FIGURE 3
The SLS printer used for the experiment.

TABLE 1 The processing parameters for the SLS printer.

Processing parameters	Setting
Laser power (W)	15
Scanning speed (mm/min)	2,500
Pre-heating target temperature (°C)	70, 80, 90, 100
Layer thickness (mm)	0.1
Machining space (*X* axis, *Y* axis and *Z* axis)	200 mm × 200 mm × 300 mm

It can be founded from the above research results that the temperature distribution on the powder bed surface during the printing process has a significant effect on the mechanical properties of the SLS printed samples. By selecting PES-HmA powder as the processing material, this research will study the influence of the pre-heating temperature distribution on the mechanical properties of the printed samples. Different from previous studies which used simulation method to analyze the temperature distribution, this manuscript proposed employing an infrared thermal imaging camera to measure the temperature distribution on the PES-HmA powder bed surface. The evaluation method of the powder bed surface temperature distribution is designed. A pre-heating setup is designed to study the performance of pre-heating temperature distribution, and its parameters will be optimized according to a response surface experiment. By analyzing the microstructure of PES-HmA samples, the influence of preheating temperature on material diffusion at the interface is investigated.

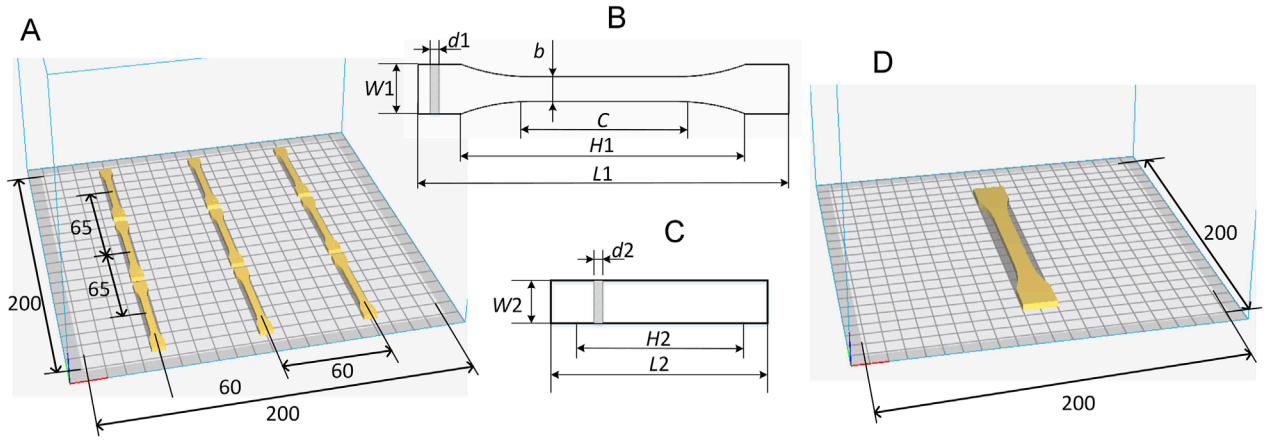

FIGURE 4
The samples printing position and its size: **(A)** pre-heating temperature distribution experiment; **(B)** tensile strength test sample; **(C)** flexural strength test sample; **(D)** pre-heating temperature experiment.

TABLE 2 The geometric dimension of the printed samples.

Symbol	Parameters	For pre-heating temperature distribution experiment (mm)	For pre-heating temperature experiment (mm)
*L*1	Total length of sample	60	150
*H*1	Length between clamps	50	115
C	Gauge length of sample	30	50
*W*1	Width at the end of sample	15	20
*d*1	Thickness of sample	3	4
b	Width at the middle parallel part	7.5	10
*L*2	Total length of sample	60	80
*H*2	Length of span between supports	50	60
*W*2	Width of sample	7.5	10
*d*2	Thickness of sample	3.5	4

2 Materials and methods

2.1 Design of pre-heating setup

Considering the SLS printing process is placed in an enclosed space, it is inconvenient to collect the powder surface temperature distribution frequently. As shown in Figure 1, a pre-heating experiment setup similar to the SLS printing chamber was designed to study the power bed surface temperature distribution. In this pre-heating setup, 4 carbon fiber heating tubes are employed as the heat source considering its high thermal efficiency. A polished stainless steel plate is designed to reflect the radiant heat from the heating tubes onto the powder bed surface. An SN-3000-WD-200 infrared temperature sensor, mounted on the top beam of the pre-heating setup, is used to detect the real-time pre-heating temperature at the center of the powder bed. It has an internal temperature calibration and compensation system. The infrared thermal emissivity of the SN-3000-WD-200 was set to 0.95, which was the same as the thermal emissivity of the PES-HmA powder used in the experiment. The object distance ratio of the SN-3000-WD-200 is 20:1, and its distance from the powder bed is 400 mm.

The working status of the carbon fiber heating tubes is controlled using the PID strategy based on the temperature detected by the infrared temperature sensor. The interactive interface is used to set the target pre-heating temperature. The position adjustment mechanism is designed to control the mounting position of the heating tubes and their stainless steel reflector. An auxiliary pre-heating plate was placed at the bottom of

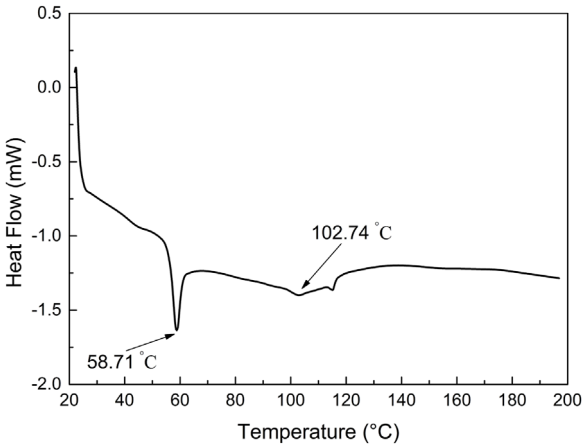

FIGURE 5
The DSC curve of PES-HmA.

the powder bed to improve the temperature uniformity on the powder surface.

In order to evaluate the performance of the designed pre-heating setup, the pre-heating area was limited in an area of 200 mm × 200 mm. The real-time temperature distribution of pre-heated powder surface was captured using the thermal imaging camera Ti400 which was produced by Fluke Thermography. The influence of heating tubes mounting position parameters (height, horizontal distance, and reflector angle, as shown in Figure 2A) on the pre-heating temperature distribution was studied by response surface experiment. A 3 factors with 3 levels (height: 50 mm, 150 mm, 250 mm; horizontal distance: 0, 30 mm, 60 mm; reflector angle: 15°, 45°, 75°) response surface experiment was designed to find the optimized parameter combination.

Ti400 captured thermal image can show the temperature value at each area of the powder bed. The average and standard deviation of the temperature value on the powder bed surface were proposed to evaluate the pre-heating characteristics. As shown in Figure 2B, the temperature value in each area of the powder bed surface is extracted from the captured thermal image named as T_i. The average temperature value of the PES-HmA powder bed surface is calculated according to Equation 1.

$$\overline{T} = \frac{\sum_{i=1}^{N} T_i}{N} \tag{1}$$

Where N is the number of temperature value that extracted from the powder bed surface thermal image.

The standard deviation of PES-HmA powder bed surface temperature is calculated according to Equation 2.

$$S = \sqrt{\frac{\sum_{i=1}^{N} \left(T_i - \overline{T}\right)}{N-1}} \tag{2}$$

2.2 The SLS printing machine and materials

After finding the optimized installation location parameters for heating tubes, the self-designed pre-heating setup will be installed on the SLS printer (as shown in Figure 3) to test its realistic manufacturing performance. The main processing parameters of the SLS printer are shown in Table 1. In order to concentrate on studying the influence of changes in the preheating temperature field on the printing performance, the laser power and scanning speed are optimized in preliminary experiments, and are set at 15 W and 2,500 mm/min respectively for all the tests in this research. PES-HmA which was purchased from Shanghai TOMIS Material Technology Co., Ltd was selected as the processing powder. The melting temperature of the selected PES-HmA is 115 °C which is lower than most polymers applied in SLS printing. The geometric appearance of the PES-HmA is irregular ellipsoids, and its diameter is normally distributed between 40 μm and 74 μm (Zhang et al., 2019b; Zhang et al., 2019a).

2.3 The evaluation of the mechanical properties

The mechanical properties of the printed samples was evaluated based on its tensile strength and flexural strength (Kam et al., 2021). To investigate the influence of pre-heating temperature distribution on the mechanical properties of the printed samples, the powder bed was divided into 9 areas, and a sample was printed in each area, as shown in Figure 4A. The mechanical properties of the samples printed in different areas were comparatively analyzed to evaluate the influence of the pre-heating temperature distribution. The geometric dimensions of the printed samples for the temperature distribution experiment is shown in Figures 4B,C and Table 2. To study the influence of pre-heating temperature on the mechanical properties of the printed samples, the sample was machined in the area as shown in Figure 4D, and its dimension is shown in Figures 4B,C and Table 2.

The tensile strength and flexural strength were tested using a microcomputer control universal testing machine, and the feed speed was controlled at 5 mm/min. The tensile strength is calculated based on Equation 3, and the flexural strength is calculated based on Equation 4.

$$\sigma_t = \frac{p}{bd} \tag{3}$$

Where p (mm) is the maximum tensile force that the sample is can withstand, b (mm) is the width of the sample, d (mm) is the thickness of the sample.

$$\sigma_f = \frac{3FL}{2bd^2} \tag{4}$$

Where F (N) is the applied force, L (mm) is the span, b (mm) is the width of the sample, d (mm) is the thickness of the sample.

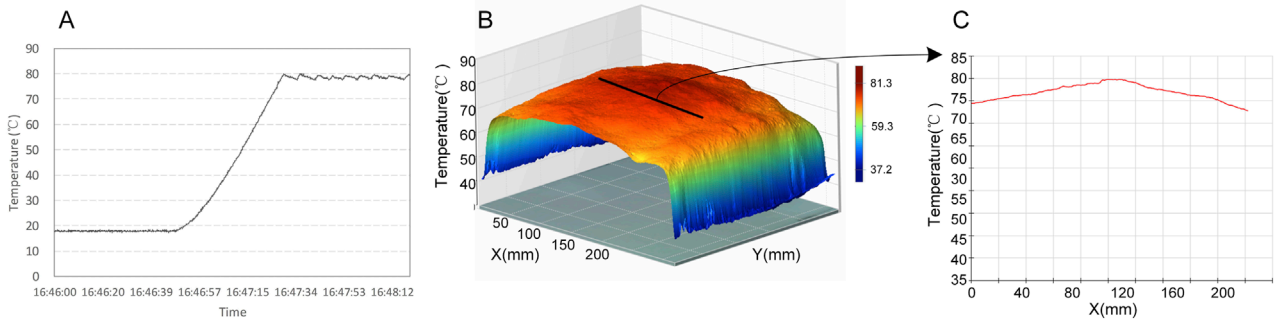

FIGURE 6
Thermal field performance: **(A)** real time temperature curve detected by SN-3000-WD-200; **(B)** Ti 400 captured thermal image in 3D diagram; **(C)** in cross-section direction.

TABLE 3 The response surface experiment results for heating tubes mounting position adjusting.

Run	Height (mm)	Distance (mm)	Angle (Degree)	Average temperature (°C)	Standard deviation
1	250	60	45	75.3	2.24
2	50	60	45	72.7	2.86
3	150	60	15	79.8	0.8
4	150	0	75	77.8	2.54
5	150	60	75	78.4	1.21
6	250	30	15	75	2.87
7	150	30	45	83.9	2.73
8	50	30	75	72.4	1.55
9	150	0	15	79.5	1.62
10	50	0	45	79.1	5.85
11	150	30	45	83.9	2.98
12	250	0	45	75	1.9
13	250	30	75	75.4	2.78
14	150	30	45	83.4	2.37
15	150	30	45	84.2	2.75
16	150	30	45	83.7	2.83
17	50	30	15	63	2.52

3 Results and discussion

3.1 The sintering property of PES-HmA

The sintering window is an important parameter to determine the sinterability of the material. In order to test the sintering property of PES-HmA, the DSC (Differential Scanning Calorimetry) curve of PES-HmA was tested using a DSC Q20 instrument. The DSC curve of PES-HmA is shown in Figure 5. It can be observed that the glass transition temperatures of PES-HmA is 58.71°C, and the sintering window is (58.71°C, 102.74°C). In the SLS process, if the pre-heating temperature is too low, the bonding between the layers is too weak to form the designed sample. If the pre-heating temperature is too high, the powder particles start to melt before the laser sintering

10.3389/fmats.2024.1480043

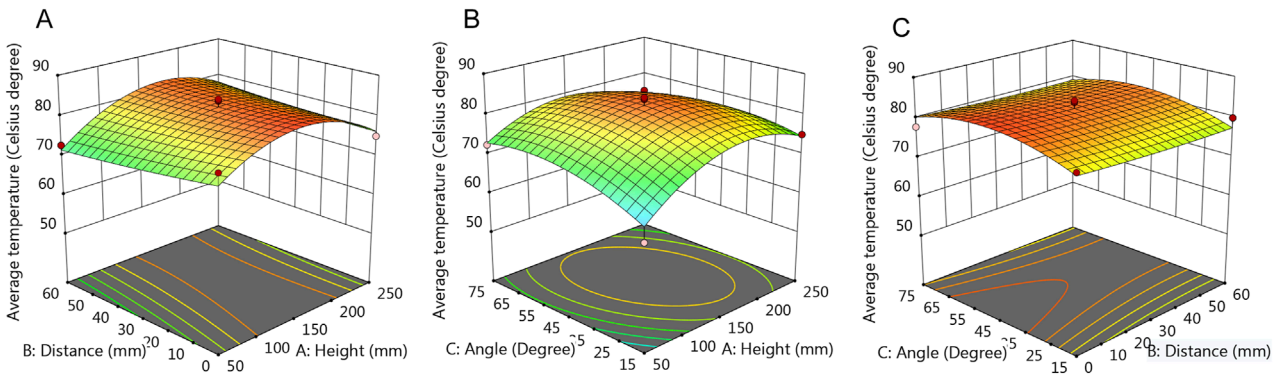

FIGURE 7
The influence of heating tubes mounting position on the average temperature of powder surface: **(A)** horizontal distance and height; **(B)** angle and height; **(C)** angle and horizontal distance.

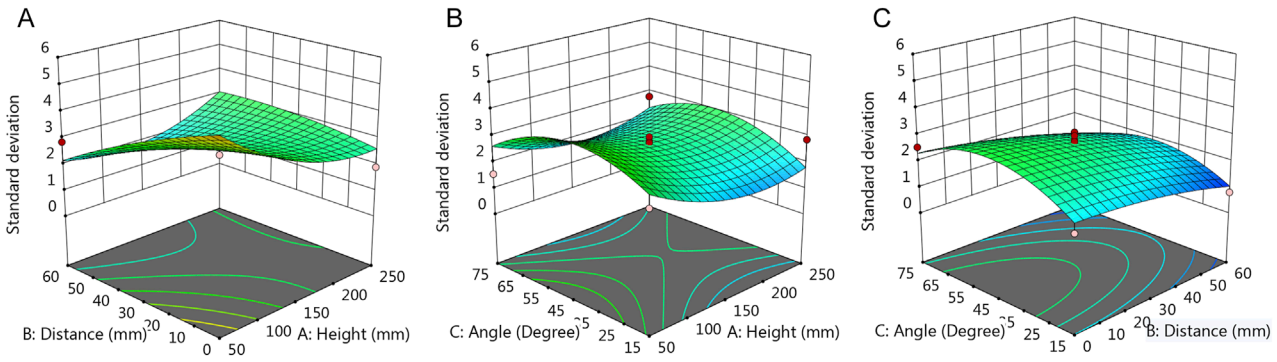

FIGURE 8
The influence of heating tubes mounting position on the standard deviation of powder surface temperature: **(A)** horizontal distance and height; **(B)** angle and height; **(C)** angle and horizontal distance.

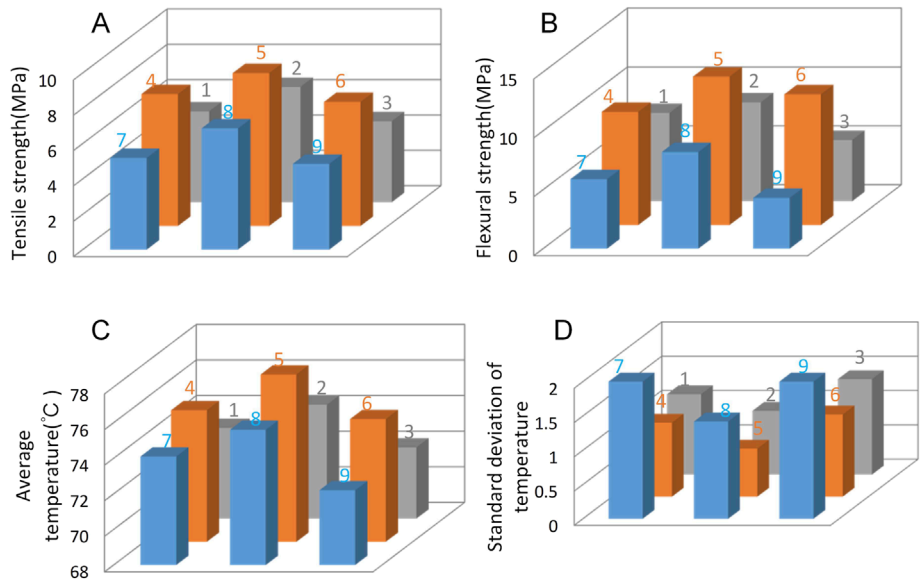

FIGURE 9
The mechanical properties of the samples printed in different areas compare with the corresponding temperature distribution in the area: **(A)** tensile strength; **(B)** flexural strength; **(C)** average temperature; **(D)** standard deviation of temperature distribution.

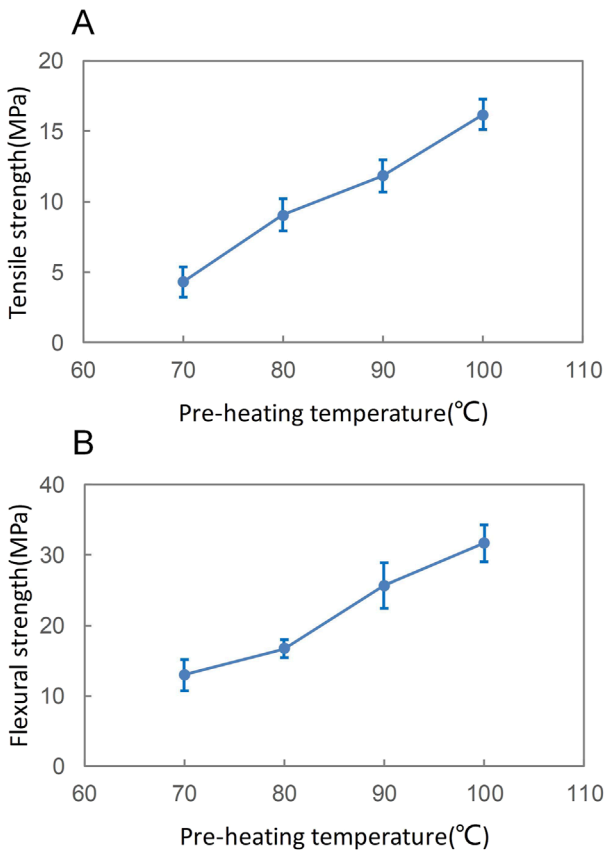

FIGURE 10
The influence of pre-heating temperature on the tensile strength and flexural strength of the printed samples: **(A)** tensile strength; **(B)** flexural strength.

process, which would affect the dimensional accuracy and quality defect of the printed sample. During the experiment, the pre-heating temperature was set between 70°C and 100°C, which is within the sintering window.

3.2 The performance of designed pre-heating setup

By setting a target pre-heating temperature, the working status of carbon fiber heating tubes would be controlled by the PID strategy. The infrared temperature sensor which was fixed on the top of the pre-heating setup would monitor the temperature at the center of the powder bed in real time, and transmit the real time temperature information to the PID control system to provide the basis for the PID control strategy. The thermal field performance was shown in Figure 6. When the target pre-heating temperature was set at 80 °C, the temperature detected by the infrared temperature sensor from the beginning of the pre-heating process is shown in Figure 6A. It can be observed that the powder bed surface temperature would increase to 80°C in 1 min from room temperature, after that it was controlled to fluctuate around 80°C by temperature PID control strategy.

In order to clearly observe the temperature difference on the powder bed surface, the surface temperature distribution on the powder bed captured by the thermal imaging camera was transformed into a 3D diagram using SmartView 3.5.31, as shown in Figure 6B. The temperature in different areas of the powder bed surface has a distinct difference. Figure 6C shows the temperature change in the cross sectional direction of the powder bed surface. On the pre-heated powder bed surface, the center obtained the highest temperature, and the surface temperature decreased with the increase of its distance from the center. It can be noted that the temperature increased by about 5°C from the edge to the center of the powder bed.

3.3 The optimization of heating tubes mounting position based on the response surface analyze

In order to study the influence of heating tubes mounting position on the powder bed surface temperature distribution, the response surface experiment was designed as shown in Table 3. Before each experiment, the heating tubes were fixed at the mounting position according to the parameters listed in Table 3. During each experiment, the target pre-heating temperature was set at 80°C, and the surface temperature distribution was captured using thermal imaging camera after the powder bed surface was pre-heated to the target temperature. After the experiment, the captured temperature distribution figure would be loaded into SmartView 3.5.31. The average temperature and the standard deviation of the temperature distribution were calculated in SmartView 3.5.31 according to Equations 1, 2, and the results are listed in Table 3.

Based on the results of response surface experiment, the influence of the heating tubes mounting position on the average temperature of the powder bed surface is shown in Figure 7. It can be observed that the height and reflector angle of the heating tube have a more significant impact on the average temperature of the powder surface compared to the horizontal distance factor. By fixing the heating tubes 150 mm above the powder bed surface, and adjusting the reflector angle to 45°, the pre-heated powder surface can obtain a higher average temperature.

The influence of the heating tubes mounting position on the standard deviation of the powder surface temperature is shown in Figure 8. It can be seen that a small standard deviation of the surface temperature can be realized when the heating tubes were fixed at a longer horizontal distance from the powder bed edge with a small reflector angle, which can be helpful to reduce the concentration of the pre-heating energy in the center of the powder bed.

3.4 The influence of pre-heating temperature on the mechanical properties

To investigate the influence of the pre-heating temperature distribution on the mechanical properties of the printed samples, the power bed was divided into 9 areas as shown in Figure 4A. A small size sample was printed in each area, and the average temperature

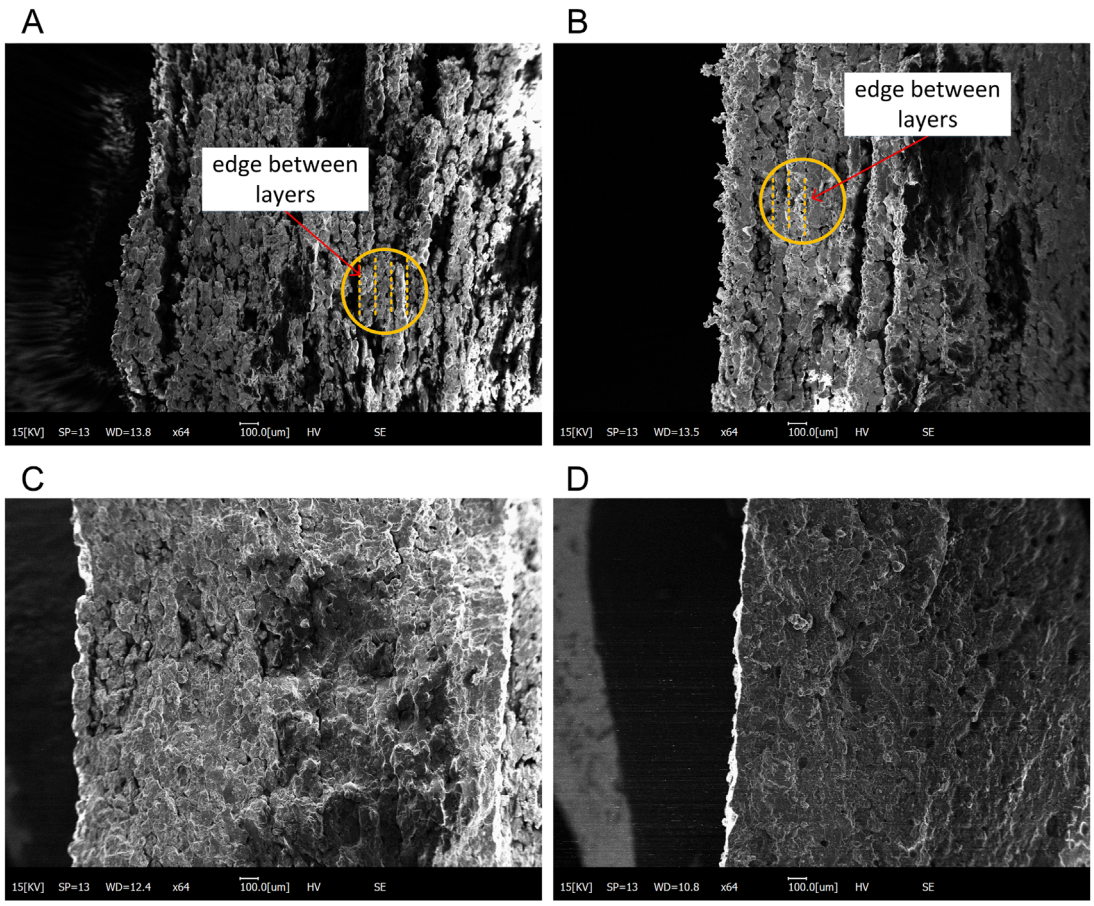

FIGURE 11
The cross-section micromorphology of the SLS samples printed in different pre-heating target temperature: **(A)** 70°C; **(B)** 80°C; **(C)** 90°C; **(D)** 100°C.

and the standard deviation of the temperature distribution in each area were calculated based on the thermal distribution image captured by the Ti400 thermal imaging camera. The tensile strength and flexural strength of each printed PES-HmA samples are shown in Figures 9A,B. It can be observed that the tensile strength of the printed sample has the same changing trend as the flexural strength of the sample printed at the same area. The average temperature and the standard deviation of the temperature distribution in each area are shown in Figures 9C,D. The area with a higher average temperature has a lower standard deviation of temperature distribution. The tensile strength and flexural strength of the printed sample are positively correlated with the average temperature in this area, and negatively correlated with the standard deviation of the pre-heating temperature in this area. The area 5 located in the center of the powder bed can draw more energy from the pre-heating tubes. Therefore, the area 5 has a higher average temperature compared to other areas. It can be noticed from Figure 9D that the temperature standard deviation of area 5 was lower than other areas, which indicates that the temperature distribution in this area is relatively uniform. The high temperature with uniform distribution is helpful for the diffusion of the particles in this area, which is conducive to improving the tensile and flexural properties of the printed sample.

In order to study the influence of pre-heating temperature on the mechanical properties of the printed samples, a standard size sample was printed in the center of the powder bed as shown in Figure 4D. The tensile strength and flexural strength of the printed samples at different pre-heating temperature were tested, and the results are shown in Figure 10. It can be found that the tensile strength and flexural strength of the printed sample would be improved with the increase of the pre-heating temperature. The higher pre-heating temperature would be helpful in improving the mechanical performance of SLS printed samples. When the pre-heating temperature was higher than 100 °C, the powder in the unprocessed area would become sticky, which was not conducive to the subsequent powder layering work.

3.5 The micromorphology analysis

By scanning the cross sectional micromorphology of the printed samples, the details of the formation process of the printed sample were investigated layer by layer at different pre-heating temperature using a scanning electron microscope (SEM). As shown in Figure 11A, when the pre-heating temperature was set at 70°C,

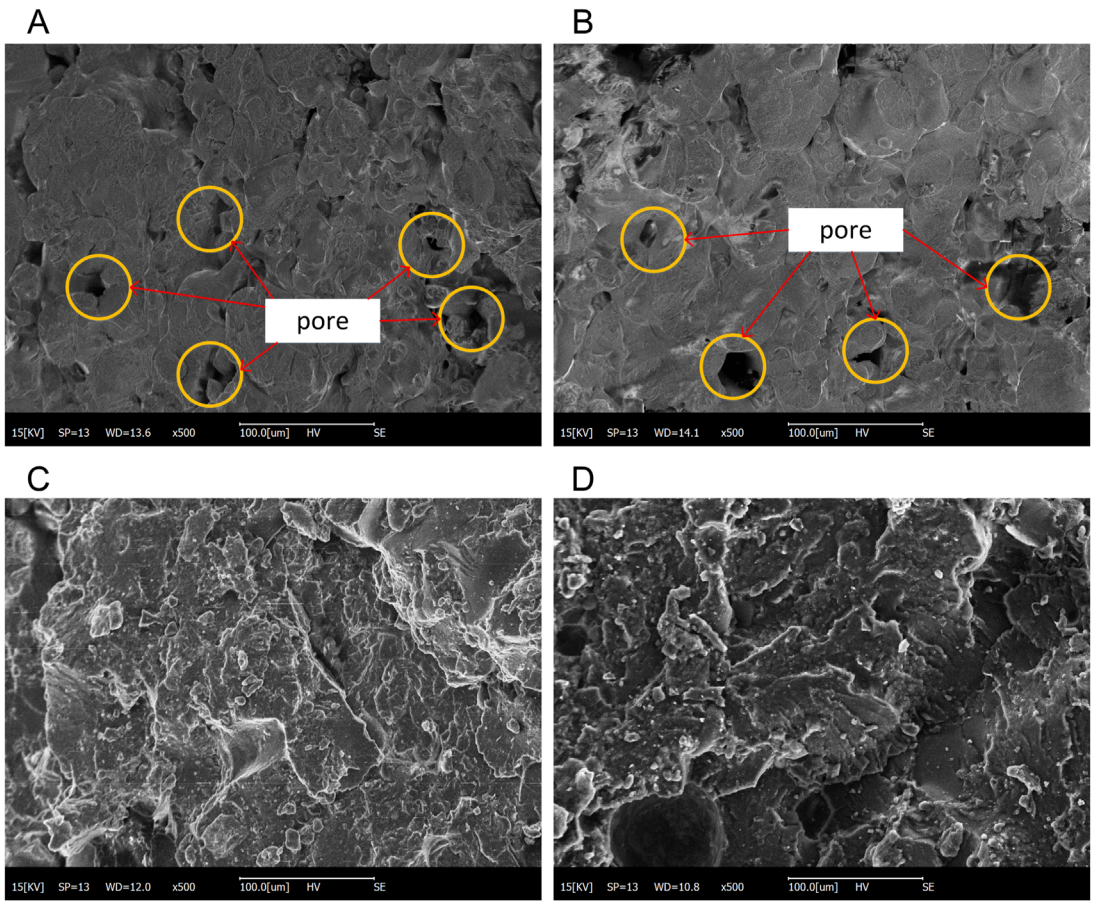

FIGURE 12
The cross-section micromorphology amplified by 500 times: **(A)** 70°C; **(B)** 80°C; **(C)** 90°C; **(D)** 100°C.

a clear distinction edge between different layers can be observed. The powder on the surface was not pre-heated enough to guarantee a good adhesion between adjacent layers, indicating that material diffusion at the layers interface was too weak. This phenomenon would reduce the mechanical properties of the printed sample. As can be seen from Figures 11B–D, with the increasing of pre-heating temperature, the edge between layers becomes tighter. The material diffusion at the layers interface was improved, which would enhance the stickiness between adjacent layers. When the pre-heating temperature higher than 90°C, the discriminating edge between different layers disappeared, and the powder in adjacent layers has a good bond with each other, which is helpful to improve the tensile strength and flexural strength of the printed samples.

As can be noticed from Figure 12, when the sample surface was amplified by 500 times, some pores could be observed when the pre-heating temperature was lower than 80°C. The temperature cannot offer enough thermal energy to help the material diffuse at the layers interface, which decreased the tensile strength and flexural strength of the printed sample. When the pre-heating temperature was higher than 90°C, the material is easy to diffuse at the layers interface. As a result, the melted powder would have closer integration, which is helpful to enhance the tensile strength and flexural strength of the printed sample.

4 Conclusion

The purpose of this study is to better understand the relationship between powder bed pre-heating performance and the mechanical properties of the printed samples. The experiment results show.

1. The pre-heating temperature distribution on the powder bed would be influenced by the mounting position of the heating tubes. A higher average temperature and lower standard deviation of the pre-heating temperature distribution can be obtained by fixing the heating tubes 150 mm above the powder bed surface, and adjusting the reflector angle to 45°.
2. The tensile strength and flexural strength of the printed sample have a positive relationship with the average temperature of the area, and a negative relationship with the standard deviation of the temperature distribution in this area.
3. By increasing the pre-heating temperature, the tensile strength and flexural strength of the printed sample can be enhanced.
4. A clear distinction edge can be noticed between different layers when the pre-heating temperature is lower than 80°C, the powder would have closer integration in adjacent layers when the pre-heating temperature was higher than 90°C, which is helpful to enhance the tensile strength and flexural strength of the printed sample.

Therefore, by rationally arranging the mounting position of the heating tubes, the uniformity of the powder bed temperature distribution can be improved, which is helpful to enhance the forming quality of the SLS process. The adjacent layers can achieve high integration by setting an appropriate pre-heating temperature. The application of this research result can improve the mechanical performance of the printed samples.

The thermal conductivity of PES-HmA powder is poor, it is very difficult to make the temperature field on the powder surface evenly distributed. It is strongly recommended for future work to do more studies on the methods of improving the thermal conductivity of PES-HmA powder, such as mixing some metal powder into it, adjusting its thermal emissivity, trying to use hot-air for preheating, *etc.*

Data availability statement

The original contributions presented in the study are included in the article/supplementary material, further inquiries can be directed to the corresponding author.

Author contributions

CG: Data curation, Investigation, Methodology, Resources, Validation, Writing–original draft, Writing–review and editing. YG: Conceptualization, Funding acquisition, Project administration, Supervision, Writing–original draft, Writing–review and editing. JL: Conceptualization, Methodology, Supervision, Writing–original draft, Writing–review and editing. YW: Investigation, Resources, Software, Writing–original draft, Writing–review and editing. JD: Data curation, Formal Analysis, Methodology, Writing–review and editing, Writing–original draft.

Funding

The author(s) declare that financial support was received for the research, authorship, and/or publication of this article. The author(s) declare that financial support was received for the research, authorship, and/or publication of this article. This work was supported by the Fundamental Research Funds for the Central Universities of China (No. 2572021BL01), National Natural Science Foundation of China (No. 52075090) and Harbin Manufacturing Technology Innovation Project (No. 2023CXRCCG009).

Conflict of interest

The authors declare that the research was conducted in the absence of any commercial or financial relationships that could be construed as a potential conflict of interest.

Publisher's note

References

Abdulhameed, O., Al-Ahmari, A., Ameen, W., and Mian, S. H. (2019). Additive manufacturing: challenges, trends, and applications. *Adv. Mech. Eng.* 11 (2), 1–27. doi:10.1177/1687814018822880

Antonov, E. N., Dunaev, A. G., Konovalov, A. N., Minaeva, S. A., and Popov, V. K. (2020). Temperature field distribution in polymer particles during surface-selective laser sintering. *Laser Phys.* 30 (5), 055601. doi:10.1088/1555-6611/ab7be3

Bai, J., Zhang, B., Song, J., Bi, G., Wang, P., and Wei, J. (2016). The effect of processing conditions on the mechanical properties of polyethylene produced by selective laser sintering. *Polym. Test.* 52, 89–93. doi:10.1016/j.polymertesting.2016.04.004

Chen, G., Suhail, S. A., Bahrami, A., Sufian, M., and Azab, M. (2023). Machine learning-based evaluation of parameters of high-strength concrete and raw material interaction at elevated temperatures. *Front. Mater.* 10, 1187094. doi:10.3389/fmats.2023.1187094

Jatti, V. S., Tamboli, S., Shaikh, S., Solke, N. S., Gulia, V., Pagac, M., et al. (2024). Optimization of tensile strength in 3D printed PLA parts via meta-heuristic approaches: a comparative study. *Front. Mater.* 10, 1336837. doi:10.3389/fmats.2023.1336837

Kam, M., İpekçi, A., and Şengül, Ö. (2021). Investigation of the effect of FDM process parameters on mechanical properties of 3D printed PA12 samples using Taguchi method. *J. Thermoplast. Compos. Mater.* 36 (1), 307–325. doi:10.1177/08927057211006459

Kruth, J. P., Mercelis, P., Van Vaerenbergh, J., Froyen, L., and Rombouts, M. (2005). Binding mechanisms in selective laser sintering and selective laser melting. *Rapid Prototyp. J.* 11 (1), 26–36. doi:10.1108/13552540510573365

Landau, E., Tiferet, E., Ganor, Y. I., Ganeriwala, R. K., Matthews, M. J., Braun, D., et al. (2020). Thermal characterization of the build chamber in electron beam melting. *Addit. Manuf.* 36, 101535. doi:10.1016/j.addma.2020.101535

Liang, K., Zhang, Q., Cao, Y., and Tang, L. (2022). Design and performance analysis of a flexible unit based on selective laser melting. *Adv. Mech. Eng.* 14 (5), 168781322210910. doi:10.1177/16878132221091008

Ling, Z., Wu, J., Wang, X., Li, X., and Zheng, J. (2018). Experimental study on the variance of mechanical properties of polyamide 6 during multi-layer sintering process in selective laser sintering. *Int. J. Adv. Manuf. Tech.* 101 (5-8), 1227–1234. doi:10.1007/s00170-018-3004-8

Liu, Q., Danlos, Y., Song, B., Zhang, B., Yin, S., and Liao, H. (2015). Effect of high-temperature preheating on the selective laser melting of yttria-stabilized zirconia ceramic. *J. Mater. Process. Technol.* 222, 61–74. doi:10.1016/j.jmatprotec.2015.02.036

Mantovani, S., Barbieri, S. G., Giacopini, M., Croce, A., Sola, A., and Bassoli, E. (2020). Synergy between topology optimization and additive manufacturing in the automotive field. *Proc. Inst. Mech. Eng. B J. Eng. Manuf.* 235 (3), 555–567. doi:10.1177/0954405420949209

Martinez, R., Todd, I., and Mumtaz, K. (2019). *In situ* alloying of elemental Al-Cu12 feedstock using selective laser melting. *Virtual. Phys. Prototyp.* 14 (3), 242–252. doi:10.1080/17452759.2019.1584402

Papadakis, L., Chantzis, D., and Salonitis, K. (2017). On the energy efficiency of pre-heating methods in SLM/SLS processes. *Int. J. Adv. Manuf. Tech.* 95 (1-4), 1325–1338. doi:10.1007/s00170-017-1287-9

Parandoush, P., and Lin, D. (2017). A review on additive manufacturing of polymer-fiber composites. *Compos. Struct.* 182, 36–53. doi:10.1016/j.compstruct.2017.08.088

Phillips, T., Fish, S., and Beaman, J. (2018). Development of an automated laser control system for improving temperature uniformity and controlling component strength in selective laser sintering. *Addit. Manuf.* 24, 316–322. doi:10.1016/j.addma.2018.10.016

Savalani, M. M., and Pizarro, J. M. (2016). Effect of preheat and layer thickness on selective laser melting (SLM) of magnesium. *Rapid Prototyp. J.* 22 (1), 115–122. doi:10.1108/rpj-07-2013-0076

Savolainen, J., and Collan, M. (2020). How additive manufacturing technology changes business models? – Review of literature. *Addit. Manuf.* 32, 101070. doi:10.1016/j.addma.2020.101070

Sharma, G. K., Pant, P., Jain, P. K., Kankar, P. K., and Tandon, P. (2020). On the suitability of induction heating system for metal additive manufacturing. *Proc. Inst. Mech. Eng. B J. Eng. Manuf.* 235 (1-2), 219–229. doi:10.1177/0954405420937854

Singh, S., Sharma, V. S., Sachdeva, A., and Sinha, S. K. (2013). Optimization and analysis of mechanical properties for selective laser sintered polyamide parts. *Mater Manuf. Process.* 28 (2), 163–172. doi:10.1080/10426914.2012.677901

Strano, G., Hao, L., Everson, R. M., and Evans, K. E. (2011). Multi-objective optimization of selective laser sintering processes for surface quality and energy saving. *Proc. Inst. Mech. Eng. B J. Eng. Manuf.* 225 (9), 1673–1682. doi:10.1177/0954405411402925

Tangestani, R., Sabiston, T., Chakraborty, A., Muhammad, W., Yuan, L., and Martin, É. (2021). An efficient track-scale model for laser powder bed fusion additive manufacturing: Part 1- thermal model. *Front. Mater.* 8, 753040. doi:10.3389/fmats.2021.753040

Yang, Z., Liu, X., Zhang, Z., Li, S., and Fang, Q. (2022). Analysis of preheating temperature field characteristics in selective laser sintering. *Adv. Mech. Eng.* 14 (1), 168781402110723. doi:10.1177/16878140211072397

Yap, C. Y., Chua, C. K., Dong, Z. L., Liu, Z. H., Zhang, D. Q., Loh, L. E., et al. (2015). Review of selective laser melting: materials and applications. *Appl. Phys. Rev.* 2 (4), 041101. doi:10.1063/1.4935926

Yuan, S., Shen, F., Chua, C. K., and Zhou, K. (2019). Polymeric composites for powder-based additive manufacturing: materials and applications. *Prog. Polym. Sci.* 91, 141–168. doi:10.1016/j.progpolymsci.2018.11.001

Zhang, H., Bourell, D., Guo, Y., Zhang, X., Zhuang, Y., Yu, Y., et al. (2019a). Study on laser sintering of pine/co-PES composites and the investment casting process. *Rapid Prototyp. J.* 25 (8), 1349–1358. doi:10.1108/rpj-01-2019-0019

Zhang, H., Guo, Y., Jiang, K., Bourell, D., Li, J., and Yu, Y. (2019b). Characterization and optimization of laser sintering copolyamide/polyether sulfone hot-melt adhesive mixtures. *Rapid Prototyp. J.* 25 (3), 614–622. doi:10.1108/rpj-12-2017-0245

Zhilyaev, I., Grieder, S., Küng, M., Brauner, C., Akermann, M., Bosshard, J., et al. (2022). Experimental and numerical analysis of the consolidation process for additive manufactured continuous carbon fiber-reinforced polyamide 12 composites. *Front. Mater.* 9, 1068261. doi:10.3389/fmats.2022.1068261